

Graphene Ink as a Conductive Templating Interlayer for Enhanced Charge Transport of C₆₀-Based Devices

D. Leonardo Gonzalez Arellano,^{*,†} Hyunbok Lee,[‡] Ethan B. Secor,[§] Edmund K. Burnett,[†] Mark C. Hersam,[§] James J. Watkins,[†] and Alejandro L. Briseno[†]

[†]Department of Polymer Science and Engineering, University of Massachusetts, Amherst, Massachusetts 01003, United States

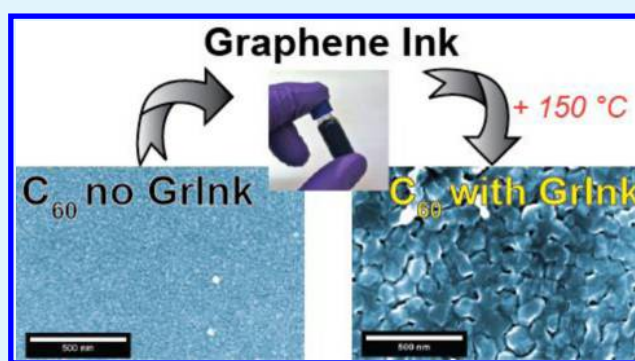
[‡]Department of Physics, Kangwon National University, 1 Gangwondaehak-gil, 24341, Republic of Korea

[§]Department of Materials Science and Engineering and Department of Chemistry, Northwestern University, Evanston, Illinois 60208, United States

S Supporting Information

ABSTRACT: We demonstrate conductive templating interlayers of graphene ink, integrating the electronic and chemical properties of graphene in a solution-based process relevant for scalable manufacturing. Thin films of graphene ink are coated onto ITO, following thermal annealing, to form a percolating network used as interlayer. We employ a benchmark n-type semiconductor, C₆₀, to study the interface of the active layer/interlayer. On bare ITO, C₆₀ molecules form films of homogeneously distributed grains; with a graphene interlayer, a preferential orientation of C₆₀ molecules is observed in the individual graphene plates. This leads to crystal growth favoring enhanced charge transport. We fabricate devices to characterize the electron injection and the effect of graphene on the device performance. We observe a significant increase in the current density with the interlayer. Current densities as high as ~ 1 mA/cm² and ~ 70 mA/cm² are realized for C₆₀ deposited with the substrate at 25 °C and 150 °C, respectively.

KEYWORDS: graphene, C₆₀, solution-processed, crystallization, templating-interlayer



INTRODUCTION

Interlayers are commonly used in organic electronics to bridge the interface between the oxide electrode and the organic active layer.^{1–3} Electron transporting layers have been shown to improve charge carrier transport by preventing the diffusion of metal atoms into the active layer and reducing the density of trap states.^{4–6} They have also been used to reduce the charge injection barrier by improving energy level alignment, typically by modifying the work function of the electrode using a thin metal oxide or employing a self-assembled monolayer.^{7–10} Interlayers have also been used to engineer the morphology of active layer films, effectively driving preferred film growth and crystal packing.^{11–14} In this regard, graphene offers the highly desirable combination of efficient charge transport and the ability to template the growth of preferred crystalline structure in organic semiconductors;¹² however, until now the existing techniques for graphene interlayer fabrication had drawbacks for large-scale manufacturing.

Many different methods for graphene production have been demonstrated with varying degrees of film quality. Mechanical exfoliation can produce high quality flakes but requires manual manipulation with limited potential for large-scale manufacturing.¹⁵ Direct epitaxial growth on SiC produces reliable, quality graphene but requires expensive wafers and high temperature

growth and is restricted to fundamental studies and applications on the original substrate.¹⁶ Molecular beam epitaxy has been used to grow chemically pure graphene with high temperature and controlled atmosphere.¹⁷ Chemical vapor deposition (CVD) yields large and uniform graphene on metal foils but requires high temperature growth and complex processing steps to transfer the as-grown graphene onto different substrates for applications.¹⁸ Oxidation of graphite and subsequent exfoliation of graphite oxide can produce large amounts of graphene oxide but introduces defects into the crystal that cannot be completely removed following reduction.^{19,20} Bottom-up synthesis from aromatic molecules²¹ and unzipping of carbon nanotubes²² have also been shown but are more expensive than alternative methods. A compelling alternative to these is the liquid-phase exfoliation of graphite,²³ shown to yield high quality graphene in a form compatible with large scale manufacturing methods such as inkjet printing,²⁴ spray coating,²⁵ and spin-coating.^{26,27}

In this work we demonstrate the use of a solution-processed graphene ink as a conductive templating interlayer for organic

Received: May 17, 2016

Accepted: October 10, 2016

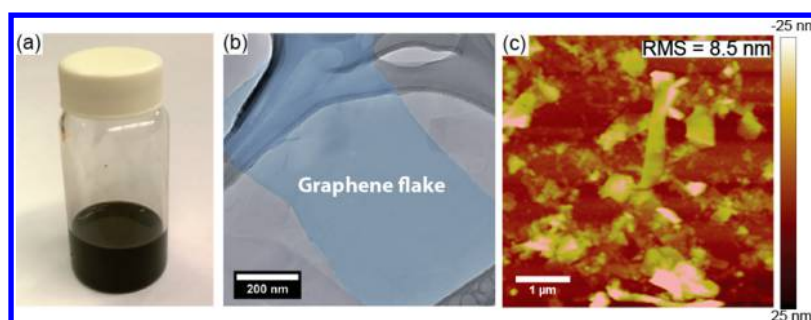


Figure 1. (a) Graphene ink “GrInk” dispersion in ethanol. (b) TEM image of an individual graphene flake on a lacey carbon grid. (c) AFM height image of GrInk film on glass and annealed.

electronic devices. To evaluate the impact of the graphene interlayer, we fabricate electron-dominated devices using the benchmark n-type semiconductor C_{60} .²⁸ In addition, C_{60} presents a suitable choice because it has been previously used as a model system for better understanding molecule–surface interactions with graphene.^{29–31}

■ GRAPHENE INK MORPHOLOGY

Graphene ink (GrInk) is obtained through the exfoliation of graphite by ultrasonication in ethanol and ethyl cellulose using the previously reported process.³² This process yields a powder containing graphene and ethyl cellulose, which can be formulated into inks with tunable viscosity and wetting properties. The ink, pictured in Figure 1a, has been described in detail in prior work, including detailed statistical analysis of the flake physical characteristics as well as Raman characterization of the material.^{24,32,33} Here we use a concentration of 10 mg/mL that consists of few-layer graphene flakes dispersed with ethyl cellulose in ethanol with typical widths of 500 nm, lengths that can reach a few micrometers, and thicknesses of ~ 2 nm. To remove aggregates existing in solution we employ sedimentation by centrifugation. Figure 1b shows a transmission electron microscopy (TEM) image obtained from a typical GrInk sample drop casted onto a lacey carbon film.

Thin films of GrInk are obtained by spin-coating onto substrates at room temperature, followed by thermal annealing at 250 °C for 30 min to obtain conductive films. Thermal annealing increases the conductivity of the GrInk films by decomposing the polymer dispersant in the ink, bringing the individual flakes into contact with each other and the substrate, yielding a conductivity of approximately 25 000 S/m as previously reported.^{24,33} The conductivity of the graphene ink films is attributed to a percolation of interconnected flakes in the vertical direction. GrInk does not need to form a uniform film to exhibit in-plane conduction; only a percolating network is required. The atomic force microscopy (AFM) height image in Figure 1c illustrates the GrInk film surface, which consists of a percolating network of graphene flakes layered on top of each other, resulting in a high RMS roughness of ~ 8.5 nm for a film with 20 nm average thickness. While the nature of the flake to flake interconnection is expected to result in resistivity higher than that of CVD-grown graphene, after thermal annealing the graphene flake network yields sufficient vertical conductivity to sustain adequate electron flow in test devices.

To obtain a series of graphene films with different thicknesses, the GrInk was diluted in ethanol and spin-coated onto half-coated ITO substrates. Following annealing of the graphene film, thermal evaporation of the subsequent layers was performed under vacuum at a base pressure of 10^{-6} mbar.

C_{60} (Puyang Huicheng Chemical Co., purity 99%) was grown with an evaporation rate of 1 Å/s. This was followed by the deposition of 10 nm of Ca at an evaporation rate of 0.1 Å/s and 100 nm of Al at an evaporation rate of 0.1 Å/s for the first 5 nm and 2 Å/s for the remainder; the dimensions of this top electrode are 2 mm². The thickness and evaporation rate of the films were monitored with a quartz crystal microbalance (QCM).

To understand the nucleation and growth behavior of C_{60} on the GrInk interlayer, we studied the changes in morphology resulting from the interlayer and growth conditions. We prepared a series of films of C_{60} with a thickness of 50 nm. Figure 2a shows the surface morphology of the control C_{60} film

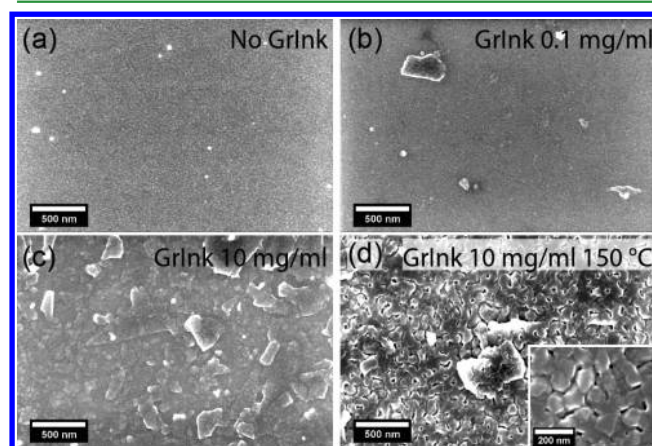


Figure 2. SEM of C_{60} films (50 nm thickness) thermally evaporated on (a) Si, (b) 0.1 mg/mL GrInk, (c) 10 mg/mL GrInk, and (d) 10 mg/mL GrInk where C_{60} was deposited with the substrate temperature held at 150 °C. Inset shows a high magnification image of the crystallites.

deposited on the bare substrate. The thin film is composed of homogeneously distributed grains of approximately 80 nm in diameter, yielding a surface roughness of $\sim 1.8 \pm 0.2$ nm and confirming that under standard deposition conditions at room temperature C_{60} forms polycrystalline films with no preferential orientation. In Figure 2b the substrate was precoated with diluted GrInk (0.1 mg/mL) and C_{60} was deposited at room temperature on top of the GrInk interlayer. The image shows that at this concentration the graphene flake density is low; therefore, morphology is very similar to that observed on the bare substrate. The few graphene flakes induce an increase in surface roughness to $\sim 11.6 \pm 3.8$ nm, and inside the individual flake a change in the C_{60} grain size can be observed. Figure 2c shows a film of C_{60} deposited on high concentration GrInk (10

mg/mL) precoated on the substrate. Here the substrate surface is completely covered by small graphene flakes in contrast with the low coverage obtained with the low concentration GrInk. This higher coverage will prove to be a critical parameter for current density enhancement, as we observe a stronger interaction between the molecules with selective areas of the surface, resulting in 2D crystallites due to the adsorption of C_{60} molecules onto individual graphene sheets, given that C_{60} has been shown to exhibit preferential growth on some carbon-based templates. As a general rule, a low supersaturation ratio is expected to yield 1D structures,^{12,34} while a higher supersaturation ratio, as in this case, produces 2D growth and the formation of isotropic bulk crystals,³⁵ which can be correlated to some of the larger 3D features randomly scattered on the surface of the film. It has also been shown in the literature that graphene presents a good surface for interaction with C_{60} molecules.^{13,31,36,37} It is possible to induce preferential growth of the crystal planes on graphene by increasing the temperature of the substrate during C_{60} evaporation. To investigate this, a set of samples was fabricated with the same parameters as before but maintaining a constant substrate temperature of 150 °C during the evaporation of C_{60} . We discovered that high substrate temperature yields larger crystallite formation, as shown in Figure 2d, in contrast to the nanocrystalline films formed during room temperature deposition. The surface roughness of these films deposited with a higher substrate temperature was measured to be 7.5 ± 1.2 nm. Reference devices prepared on ITO substrates at high temperature show an increase in grain size, which could potentially yield an increase in device performance; however, as shown in Figure S1, the crystallites do not cover the entire surface of the device, as opposed to the case where 10 mg/mL GrInk is used where full coverage is achieved, and could cause leakage current in the device.

EFFECT OF THE GRAPHENE TEMPLATE ON C_{60} CRYSTALLINITY

To assess the crystallization behavior that the C_{60} films exhibit when deposited on the GrInk interlayers, grazing incidence X-ray diffraction (GIXD) scattering was carried out. Figure 3a

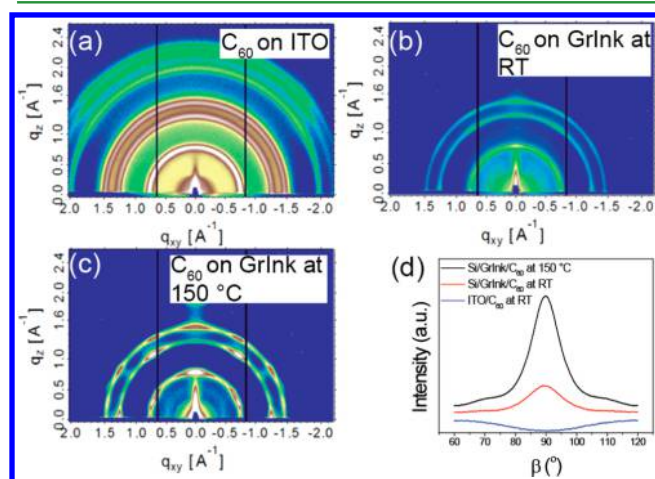


Figure 3. GIXD maps of C_{60} films deposited on top of (a) ITO, (b) 20 nm thick GrInk film at room temperature during deposition, and (c) 20 nm thick GrInk at 150 °C during deposition. (d) Approximate pole figures of the (111) Bragg reflection of C_{60} under differing processing conditions.

shows GIXD results for a thermally evaporated thin film of C_{60} on a bare ITO substrate (no surface treatment, no GrInk). The sample shows broad diffraction rings, which indicate a crystalline film with no preferred orientation. The C_{60} exhibits an fcc crystal packing motif, as seen in previous literature, with the diffraction rings at q -values of 0.75 \AA^{-1} , 1.25 \AA^{-1} , and 1.5 \AA^{-1} corresponding to (111), (220), and (311) indices, respectively.^{6,38,39} When C_{60} is deposited on a $\text{SiO}_2/\text{GrInk}$ substrate, corresponding to Figure 3b, the Bragg reflections are still present at the same q -values but indicate an alignment of the (111) plane parallel to the substrate. When the C_{60} is deposited on a heated $\text{SiO}_2/\text{GrInk}$ substrate, these reflections increase in intensity while also azimuthally narrowing, as shown in Figure 3c. Holding the ITO substrate at 150 °C without a GrInk interlayer does not change the degree of crystallinity as shown in Figure S1b. The heated substrate increases the crystallinity of the C_{60} film while keeping the (111) plane oriented parallel to the substrate. To further examine the effect of a heated substrate on the crystal orientation, we used the (111) peak to estimate the crystal orientation distribution. Figure 3d shows an angular full width at half-maximum (fwhm) of 13.4° and 12.1° corresponding to deposition on GrInk surfaces at room temperature and 150 °C, respectively. We note that the narrowing of the angular spread corresponding to the heated substrate indicates that the crystalline domains are more aligned out-of-plane.^{7,40}

ELECTRON-DOMINATED DEVICE CHARACTERIZATION

To quantify the impact that these morphology changes have on charge transport, we carried out measurements on a series of electron-dominated devices prepared on ITO/glass substrates. The device configuration is shown in Figure 4a, depicting a 200 nm thick C_{60} film evaporated on top of a GrInk interlayer of different thicknesses followed by the evaporation of Ca (10 nm) and Al (100 nm) as the top electrode.

The measured current density–voltage (J – V) characteristics of these devices were obtained with a Keithley 4200-SCS at room temperature under dark conditions, immediately following metal deposition. The devices were characterized following standard procedures for electron-dominated devices.^{41–43} The J – V characteristics are presented in a log–log scale in Figure 4b and indicate a significant enhancement in the current density when GrInk is inserted as an interlayer. Moreover, a relationship between the increase in charge injection and the concentration of the interlayer is observed. With a 0.1 mg/mL interlayer, the low voltage behavior of the devices is similar to the reference of pristine C_{60} , and as the voltage increases, the current density also increases, showing close to 1 order of magnitude increase in current density in comparison with the reference. As the concentration of the GrInk interlayer increases, a continuous increase in the current density is observed. The graphene ink concentration and the interlayer thickness can also be related to the total coverage of graphene flakes on the surface, as shown in Figure 2; this offers a suitable surface for increase in crystallinity of C_{60} and as a result an increase in current density. For reference, a plot of the rectification behavior of the ITO device and the most concentrated GrInk interlayer is shown in Figure S2. The squares in Figure 4c illustrate this trend, showing the current density of devices at 6 V. The incorporation of a GrInk interlayer leads to an increase in current density of up to 3 orders of magnitude compared to the reference device. The

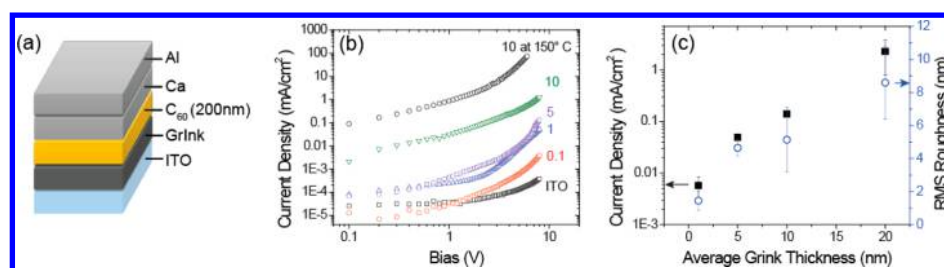


Figure 4. (a) Schematic illustration of the device configuration of electron-dominated device consisting of Al (100 nm)/Ca (10 nm)/C₆₀ (200 nm)/GrInk (variable thickness)/ITO. (b) *J*–*V* characteristics of devices prepared at room temperature, with GrInk varying interlayer concentrations, ITO (no interlayer, black squares), 0.1 mg/mL (red circles), 1 mg/mL (blue upward triangles), 5 mg/mL (purple squares), 10 mg/mL (green downward triangles), and 10 mg/mL with the substrate held at 150 °C during C₆₀ evaporation (black circles). (c) Squares, comparison of the measured current density of electron-dominated devices at 6 V against the resistivity of the films as a function of GrInk interlayer average thickness; circles, evolution of surface roughness of C₆₀/GrInk films as a function of GrInk interlayer average thickness. An average of at least six devices was used for statistical analysis.

highest current density is consistently measured in the devices with higher concentrations of GrInk which have an average thickness of 20 nm, reaching values of ~ 1 mA/cm².

The increase in current density can be correlated to the enhanced crystalline order of the films, as corroborated by GIXD measurements. It has been previously shown that increased crystal orientation in organic materials leads to higher current flow.^{44,45} Taken together, these results show that the GrInk interlayer promotes more crystalline domains, which are correlated with the measured increase in current densities in devices with thicker GrInk layers. This is reinforced by results from devices prepared by C₆₀ deposition onto a 150 °C GrInk film, which showed increased crystalline orientation. In this case, the current density reaches a maximum value of ~ 70 mA/cm² at 6 V, over 1 order of magnitude higher than that of devices prepared at room temperature.

These results are in agreement with the changes observed in surface roughness of the films as a function of GrInk thickness. The relationship between surface roughness and average GrInk interlayer thickness is depicted as circles in Figure 4c and show a similar trend compared to the current density increase. For a thin film of GrInk, the RMS surface roughness is comparable to that of the substrate at 1.5 ± 0.5 nm. However, as the average GrInk thickness increases, the roughness also increases gradually to 4.7 ± 0.5 nm and 5.1 ± 2 for 5 and 10 nm films, respectively, finally reaching a maximum value of 8.6 ± 2.2 nm for samples with an average GrInk thickness of 20 nm, corresponding to the highest concentration of GrInk. Previous work on graphene shows that it induces epitaxial growth of organic adsorbate molecules.^{12,46} In the particular case of C₆₀, graphene has been shown to promote crystal growth in preferential orientations due to strong epitaxial relation between C₆₀ crystal and graphene.^{13,29} In the particular case of GrInk, we obtain films with a rough topography and surface roughness and interfaces are known to promote and enhance crystal nucleation.⁴⁷ The two effects enhance the total crystal quality and nucleation density, respectively. We note that the roughness of the 20 nm GrInk film is maintained even when C₆₀ is deposited at higher temperatures (8.6 ± 2.7 nm); however, the increase in current density indicates that the higher crystalline order is the main driving factor for the change in device performance.

CONCLUSION

We have demonstrated a solution-processed graphene film as an effective interlayer in organic devices, which shows great

promise for large scale manufacturing techniques. The combination of AFM and GIXD measurements provides an understanding of the effect of the graphene ink interlayer on the growth mode and crystalline ordering of C₆₀ deposited via vacuum evaporation. It is observed that C₆₀ deposited on a network of graphene flakes results in highly crystalline domains. To quantify the effect of these morphological changes on charge transport, we tested a series of electron-dominated devices, revealing a significant enhancement in charge transport as a result of the GrInk interlayer. Ongoing studies include the extension of these results to large-area flexible devices for use in applications, such as sensors, and energy-related devices, such as batteries and supercapacitors.

ASSOCIATED CONTENT

Supporting Information

The Supporting Information is available free of charge on the ACS Publications website at DOI: 10.1021/acsami.6b05536.

Analysis of C₆₀ deposited at 150 °C. *J*–*V* characteristics of devices with maximum concentration of GrInk and no GrInk (PDF)

AUTHOR INFORMATION

Corresponding Author

*E-mail: dlga@mail.pse.umass.edu.

Notes

The authors declare no competing financial interest.

ACKNOWLEDGMENTS

Partial fellowship support for L.G.A was provided by the Consejo Nacional de Ciencia y Tecnología (CONACyT), México. The GIXD measurements were carried out by Feng Liu at the Stanford Synchrotron Radiation Light Source. A.L.B. and J.J.W. thank the Center for Hierarchical Manufacturing (CMMI-0531171). A.L.B. thanks the NSF (DMR-1508627). E.B.S. and M.C.H. acknowledge the Office of Naval Research (N00014-11-1-0690) and the Air Force Research Laboratory (FA8650-15-2-5518). The U. S. Government is authorized to reproduce and distribute reprints for Governmental purposes notwithstanding any copyright notation thereon. The views and conclusions contained herein are those of the authors and should not be interpreted as necessarily representing the official policies or endorsements, either expressed or implied, of the sponsors.

REFERENCES

- (1) Ishii, H.; Sugiyama, K.; Ito, E.; Seki, K. Energy Level Alignment and Interfacial Electronic Structures at Organic/Metal and Organic/Organic Interfaces. *Adv. Mater.* **1999**, *11*, 605–625.
- (2) Garcia, A.; Bakus, R. C., II; Zalar, P.; Hoven, C. V.; Brzezinski, J. Z.; Nguyen, T.-Q. Controlling Ion Motion in Polymer Light-Emitting Diodes Containing Conjugated Polyelectrolyte Electron Injection Layers. *J. Am. Chem. Soc.* **2011**, *133*, 2492–2498.
- (3) Hoven, C.; Yang, R.; Garcia, A.; Heeger, A. J.; Nguyen, T.-Q.; Bazan, G. C. Ion Motion in Conjugated Polyelectrolyte Electron Transporting Layers. *J. Am. Chem. Soc.* **2007**, *129*, 10976–10977.
- (4) Wang, N.; Yu, J.; Zang, Y.; Huang, J.; Jiang, Y. Effect of Buffer Layers on the Performance of Organic Photovoltaic Cells Based on Copper Phthalocyanine and C₆₀. *Sol. Energy Mater. Sol. Cells* **2010**, *94*, 263–266.
- (5) Hong, Z.; Xiaoman, C.; Haijun, T.; Geng, Z. Enhanced Performance of C₆₀ Organic Field Effect Transistors Using a Tris(8-Hydroxyquinoline) Aluminum Buffer Layer. *J. Semicond.* **2011**, *32*, 094005.
- (6) Yang, J.-P.; Sun, Q.-J.; Yonezawa, K.; Hinderhofer, A.; Gerlach, A.; Broch, K.; Bussolotti, F.; Gao, X.; Li, Y.; Tang, J.; Schreiber, F.; Ueno, N.; Wang, S.-D.; Kera, S. Interface Optimization Using Diindenoperylene for C₆₀ Thin Film Transistors with High Electron Mobility and Stability. *Org. Electron.* **2014**, *15*, 2749–2755.
- (7) Lee, H.; Puodziukynaite, E.; Zhang, Y.; Stephenson, J. C.; Richter, L. J.; Fischer, D. A.; DeLongchamp, D. M.; Emrick, T.; Briseno, A. L. Poly(sulfobetaine methacrylate)s as Electrode Modifiers for Inverted Organic Electronics. *J. Am. Chem. Soc.* **2015**, *137*, 540–549.
- (8) Akaike, K.; Koch, N.; Oehzelt, M. Fermi Level Pinning Induced Electrostatic Fields and Band Bending at Organic Heterojunctions. *Appl. Phys. Lett.* **2014**, *105*, 223303.
- (9) Greiner, M. T.; Helander, M. G.; Tang, W.-M.; Wang, Z.-B.; Qiu, J.; Lu, Z.-H. Universal Energy-Level Alignment of Molecules on Metal Oxides. *Nat. Mater.* **2012**, *11*, 76–81.
- (10) Lee, H.; Cho, S. W.; Han, K.; Jeon, P. E.; Whang, C.-N.; Jeong, K.; Cho, K.; Yi, Y. The Origin of the Hole Injection Improvements at Indium Tin Oxide/Molybdenum Trioxide/N,N'-Bis(1-Naphthyl)-N,N'-Diphenyl-1,1'-Biphenyl-4,4'-Diamine Interfaces. *Appl. Phys. Lett.* **2008**, *93*, 43308–43308.
- (11) Itaka, K.; Yamashiro, M.; Yamaguchi, J.; Haemori, M.; Yaginuma, S.; Matsumoto, Y.; Kondo, M.; Koinuma, H. High-Mobility C₆₀ Field-Effect Transistors Fabricated on Molecular-Wetting Controlled Substrates. *Adv. Mater.* **2006**, *18*, 1713–1716.
- (12) Zhang, Y.; Diao, Y.; Lee, H.; Mirabito, T. J.; Johnson, R. W.; Puodziukynaite, E.; John, J.; Carter, K. R.; Emrick, T.; Mannsfeld, S. C. B.; Briseno, A. L. Intrinsic and Extrinsic Parameters for Controlling the Growth of Organic Single-Crystalline Nanopillars in Photovoltaics. *Nano Lett.* **2014**, *14*, 5547–5554.
- (13) Jung, M.; Shin, D.; Sohn, S.-D.; Kwon, S.-Y.; Park, N.; Shin, H.-J. Atomically Resolved Orientational Ordering of C₆₀ Molecules on Epitaxial Graphene on Cu(111). *Nanoscale* **2014**, *6*, 11835–11840.
- (14) Ahn, K.; Beom Kim, J.; Park, H.; Kim, H.; Hyung Lee, M.; Joon Kim, B.; Ho Cho, J.; Sung Kang, M.; Ryeol Lee, D. Enhancing Crystallinity of C₆₀ Layer by Thickness-Control of Underneath Pentacene Layer for High Mobility C₆₀/Pentacene Ambipolar Transistors. *Appl. Phys. Lett.* **2013**, *102*, 043306.
- (15) Park, S.; Ruoff, R. S. Chemical Methods for the Production of Graphenes. *Nat. Nanotechnol.* **2009**, *4*, 217–224.
- (16) Forbeaux, I.; Themlin, J. M.; Debever, J. M. Heteroepitaxial Graphite on 6 H– Sic (0001): Interface Formation through Conduction-Band Electronic Structure. *Phys. Rev. B: Condens. Matter Mater. Phys.* **1998**, *58*, 16396–16406.
- (17) Hackley, J.; Ali, D.; DiPasquale, J.; Demaree, J.; Richardson, C. Graphitic Carbon Growth on Si (111) Using Solid Source Molecular Beam Epitaxy. *Appl. Phys. Lett.* **2009**, *95*, 133114.
- (18) Li, X.; Cai, W.; An, J.; Kim, S.; Nah, J.; Yang, D.; Piner, R.; Velamakanni, A.; Jung, I.; Tutuc, E.; Banerjee, S. K.; Colombo, L.; Ruoff, R. S. Large-Area Synthesis of High-Quality and Uniform Graphene Films on Copper Foils. *Science* **2009**, *324*, 1312–1314.
- (19) Dreyer, D. R.; Park, S.; Bielawski, C. W.; Ruoff, R. S. The Chemistry of Graphene Oxide. *Chem. Soc. Rev.* **2010**, *39*, 228–240.
- (20) Stankovich, S.; Dikin, D. A.; Piner, R. D.; Kohlhaas, K. A.; Kleinhammes, A.; Jia, Y.; Wu, Y.; Nguyen, S. T.; Ruoff, R. S. Synthesis of Graphene-Based Nanosheets Via Chemical Reduction of Exfoliated Graphite Oxide. *Carbon* **2007**, *45*, 1558–1565.
- (21) Matei, D. G.; Weber, N. E.; Kurasch, S.; Wundrack, S.; Woszczyzna, M.; Grothe, M.; Weimann, T.; Ahlers, F.; Stosch, R.; Kaiser, U.; Turchanin, A. Functional Single-Layer Graphene Sheets from Aromatic Monolayers. *Adv. Mater.* **2013**, *25*, 4146–4151.
- (22) Jiao, L.; Zhang, L.; Wang, X.; Diankov, G.; Dai, H. Narrow Graphene Nanoribbons from Carbon Nanotubes. *Nature* **2009**, *458*, 877–880.
- (23) Blake, P.; Brimicombe, P. D.; Nair, R. R.; Booth, T. J.; Jiang, D.; Schedin, F.; Ponomarenko, L. A.; Morozov, S. V.; Gleeson, H. F.; Hill, E. W.; Geim, A. K.; Novoselov, K. S. Graphene-Based Liquid Crystal Device. *Nano Lett.* **2008**, *8*, 1704–1708.
- (24) Secor, E. B.; Prabhuramirashi, P. L.; Puntambekar, K.; Geier, M. L.; Hersam, M. C. Inkjet Printing of High Conductivity, Flexible Graphene Patterns. *J. Phys. Chem. Lett.* **2013**, *4*, 1347–1351.
- (25) Kim, D.-Y.; Sinha-Ray, S.; Park, J.-J.; Lee, J.-G.; Cha, Y.-H.; Bae, S.-H.; Ahn, J.-H.; Jung, Y. C.; Kim, S. M.; Yarin, A. L.; Yoon, S. S. Self-Healing Reduced Graphene Oxide Films by Supersonic Kinetic Spraying. *Adv. Funct. Mater.* **2014**, *24*, 4986–4995.
- (26) Yamaguchi, H.; Eda, G.; Mattevi, C.; Kim, H.; Chhowalla, M. Highly Uniform 300 Mm Wafer-Scale Deposition of Single and Multilayered Chemically Derived Graphene Thin Films. *ACS Nano* **2010**, *4*, 524–528.
- (27) Becerril, H. A.; Mao, J.; Liu, Z.; Stoltenberg, R. M.; Bao, Z.; Chen, Y. Evaluation of Solution-Processed Reduced Graphene Oxide Films as Transparent Conductors. *ACS Nano* **2008**, *2*, 463–470.
- (28) Hummelen, J. C.; Knight, B. W.; LePeq, F.; Wudl, F.; Yao, J.; Wilkins, C. L. Preparation and Characterization of Fulleroid and Methanofullerene Derivatives. *J. Org. Chem.* **1995**, *60*, 532–538.
- (29) Cho, J.; Smerdon, J.; Gao, L.; Süzer, Ö.; Guest, J. R.; Guisinger, N. P. Structural and Electronic Decoupling of C₆₀ from Epitaxial Graphene on Sic. *Nano Lett.* **2012**, *12*, 3018–3024.
- (30) Ulbricht, H.; Moos, G.; Hertel, T. Interaction of C₆₀ with Carbon Nanotubes and Graphite. *Phys. Rev. Lett.* **2003**, *90*, 095501.
- (31) Kim, K.; Lee, T. H.; Santos, E. J.; Jo, P. S.; Salleo, A.; Nishii, Y.; Bao, Z. Structural and Electrical Investigation of C₆₀-Graphene Vertical Heterostructures. *ACS Nano* **2015**, *9*, 5922–5928.
- (32) Liang, Y. T.; Hersam, M. C. Highly Concentrated Graphene Solutions Via Polymer Enhanced Solvent Exfoliation and Iterative Solvent Exchange. *J. Am. Chem. Soc.* **2010**, *132*, 17661–17663.
- (33) Secor, E. B.; Ahn, B. Y.; Gao, T. Z.; Lewis, J. A.; Hersam, M. C. Rapid and Versatile Photonic Annealing of Graphene Inks for Flexible Printed Electronics. *Adv. Mater.* **2015**, *27*, 6683–6688.
- (34) Meshot, E. R.; Patel, K. D.; Tawfick, S.; Juggernaut, K. A.; Bedewy, M.; Verploegen, E. A.; De Volder, M. F. L.; Hart, A. J. Photoconductive Hybrid Films Via Directional Self-Assembly of C₆₀ on Aligned Carbon Nanotubes. *Adv. Funct. Mater.* **2012**, *22*, 577–584.
- (35) Shin, H. S.; Yoon, S. M.; Tang, Q.; Chon, B.; Joo, T.; Choi, H. C. Highly Selective Synthesis of C₆₀ Disks on Graphite Substrate by a Vapor–Solid Process. *Angew. Chem., Int. Ed.* **2008**, *47*, 693–696.
- (36) Li, G.; Zhou, H. T.; Pan, L. D.; Zhang, Y.; Mao, J. H.; Zou, Q.; Guo, H. M.; Wang, Y. L.; Du, S. X.; Gao, H.-J. Self-Assembly of C₆₀ Monolayer on Epitaxially Grown, Nanostructured Graphene on Ru(0001) Surface. *Appl. Phys. Lett.* **2012**, *100*, 013304.
- (37) Chen, M.; Zhou, H.; Yu, F.; Yang, H.; Wang, G.; He, J.; Sun, L. Tuning the Layer-Dependent Doping Effect of Graphenes by C₆₀. *Nanoscale* **2013**, *5*, 8359–8362.
- (38) de Boer, J. L.; van Smaalen, S.; Petricek, V.; Dusek, P. M.; Verheijen, M. A.; Meijer, G. Hexagonal Close-Packed C₆₀. *Chem. Phys. Lett.* **1994**, *219*, 469–472.
- (39) Hinderhofer, A.; Gerlach, A.; Broch, K.; Hosokai, T.; Yonezawa, K.; Kato, K.; Kera, S.; Ueno, N.; Schreiber, F. Geometric and Electronic Structure of Templated C₆₀ on Diindenoperylene Thin Films. *J. Phys. Chem. C* **2013**, *117*, 1053–1058.

(40) Wise, A.; Zhang, Y.; Fan, J.; Wudl, F.; Briseno, A.; Barnes, M. Spectroscopy of Discrete Vertically Oriented Single-Crystals of N-Type Tetraazaterrylene: Understanding the Role of Defects in Molecular Semiconductor Photovoltaics. *Phys. Chem. Chem. Phys.* **2014**, *16*, 15825–15830.

(41) Mandoc, M. M.; de Boer, B.; Blom, P. W. M. Electron-Only Diodes of Poly(Dialkoxy-P-Phenylene Vinylene) Using Hole-Blocking Bottom Electrodes. *Phys. Rev. B: Condens. Matter Mater. Phys.* **2006**, *73*, 155205.

(42) Crone, B.; Campbell, I.; Davids, P.; Smith, D. Charge Injection and Transport in Single-Layer Organic Light-Emitting Diodes. *Appl. Phys. Lett.* **1998**, *73*, 3162–3164.

(43) Palilis, L. C.; Uchida, M.; Kafafi, Z. H. Electron Injection in "Electron-Only" Devices Based on a Symmetric Metal/Silole/Metal Structure. *IEEE J. Sel. Top. Quantum Electron.* **2004**, *10*, 79–88.

(44) Lee, W. Y.; Giri, G.; Diao, Y.; Tassone, C. J.; Matthews, J. R.; Sorensen, M. L.; Mannsfeld, S. C. B.; Chen, W. C.; Fong, H. H.; Tok, J. B. H.; Toney, M. F.; He, M. Q.; Bao, Z. A. Effect of Non-Chlorinated Mixed Solvents on Charge Transport and Morphology of Solution-Processed Polymer Field-Effect Transistors. *Adv. Funct. Mater.* **2014**, *24*, 3524–3534.

(45) Diao, Y.; Tee, B. C. K.; Giri, G.; Xu, J.; Kim, D. H.; Becerril, H. A.; Stoltenberg, R. M.; Lee, T. H.; Xue, G.; Mannsfeld, S. C. B.; Bao, Z. Solution Coating of Large-Area Organic Semiconductor Thin Films with Aligned Single-Crystalline Domains. *Nat. Mater.* **2013**, *12*, 665–671.

(46) Wang, Q. H.; Hersam, M. C. Room-Temperature Molecular-Resolution Characterization of Self-Assembled Organic Monolayers on Epitaxial Graphene. *Nat. Chem.* **2009**, *1*, 206–211.

(47) Briseno, A. L.; Mannsfeld, S. C. B.; Ling, M. M.; Liu, S.; Tseng, R. J.; Reese, C.; Roberts, M. E.; Yang, Y.; Wudl, F.; Bao, Z. Patterning Organic Single-Crystal Transistor Arrays. *Nature* **2006**, *444*, 913–917.